J Membrane Biol (2010) 236:3–13
DOI 10.1007/s00232-010-9279-9

ORIGINAL ARTICLES

Induced Transmembrane Voltage and Its Correlation with Electroporation-Mediated Molecular Transport

Tadej Kotnik · Gorazd Pucihar · Damijan Miklavčič

Received: 30 December 2009 / Accepted: 11 June 2010 / Published online: 9 July 2010

Abstract Exposure of a cell to an electric field results in inducement of a voltage across its membrane (induced transmembrane voltage, $\Delta\Psi_m$) and, for sufficiently strong fields, in a transient increase of membrane permeability (electroporation). We review the analytical, numerical and experimental methods for determination of $\Delta\Psi_m$ and a method for monitoring of transmembrane transport. We then combine these methods to investigate the correlation between $\Delta\Psi_m$ and molecular transport through an electroporated membrane for isolated cells of regular and irregular shapes, for cells in dense suspensions as well as for cells in monolayer clusters. Our experiments on isolated cells of both regular and irregular shapes confirm the theoretical prediction that the highest absolute values of $\Delta\Psi_m$ are found in the membrane regions facing the electrodes and that electroporation-mediated transport is confined to these same regions. For cells in clusters, the location of transport regions implies that, at the field strengths sufficient for electroporation, the cells behave as electrically insulated (i.e., as individual) cells. In contrast, with substantially weaker, nonelectroporating fields, potentiometric measurements show that the cells in these same clusters behave as electrically interconnected cells (i.e., as one large cell). These results suggest that sufficiently high electric fields affect the intercellular pathways and thus alter the electric behavior of the cells with respect to their normal physiological state.

T. Kotnik · G. Pucihar (✉) · D. Miklavčič
Department of Biomedical Engineering, Faculty of Electrical Engineering, University of Ljubljana, Tržaška 25, 1000 Ljubljana, Slovenia
e-mail: gorazd.pucihar@fe.uni-lj.si

Keywords Induced transmembrane voltage · Electroporation · Transmembrane transport · Isolated cell · Cell suspension · Cell cluster · Di-8-ANEPPS · Propidium iodide

Introduction

Under physiological conditions, the cell plasma membrane is subjected to a voltage (electric potential difference) caused by a system of ion pumps and channels in the membrane. This voltage, termed the *resting transmembrane voltage*, is in the range of tens of millivolts and is present in practically every cell from the simplest prokaryotes to mammalian cells (Alberts et al. 2008; Lodish et al. 2008). As a consequence, the plasma membrane is well adapted to the physiological ranges of transmembrane voltage, the mechanical pressure exerted by it and the capacitive energy it stores in the membrane.

Exposure of a cell to an external electric field results in an additional component of the voltage across the membrane. This component, termed the *induced transmembrane voltage* (also *induced membrane voltage* or *induced transmembrane potential difference*) and denoted by $\Delta\Psi_m$, is superimposed onto the resting voltage and exists only as long as the external field is present. The induced transmembrane voltage is proportional to the strength of the external electric field, and consequently exposures to sufficiently strong fields can lead to transmembrane voltages far exceeding their physiological range (Pauly and Schwan 1959; Grosse and Schwan 1992; Kotnik et al. 1997; Kotnik and Miklavčič, 2000a; Gimsa and Wachner 2001; Pucihar et al. 2006; Hu and Joshi 2009). This can also lead to nonphysiological effects, including structural rearrangements of lipids in the membrane bilayer resulting in formation and stabilization of pores. This

phenomenon is termed *electroporation*, or *electropermeabilization*, and permits transmembrane transport of molecules for which an intact membrane is poorly permeable (Neumann and Rosenheck 1972; Weaver 2003; Teissié et al. 2005; Escoffre et al. 2009).

Many studies imply that electroporation and the resulting molecular flow across the membrane are limited to the regions of the membrane exposed to a sufficiently high $\Delta\Psi_m$ (Hibino et al. 1991, 1993; Tekle et al. 1994; Gabriel and Teissié 1997, 1999; Kennedy et al. 2008). Although the processes of formation and stabilization of each pore in the membrane are stochastic, on the scale of cells and tissues the effects of membrane electroporation only become detectable at $\Delta\Psi_m$ exceeding a certain "critical" value. This value can range from $\sim$250 mV up to 1 V, depending on the duration of the exposure, experimental conditions, the sensitivity of the detection method and the cell type (Hibino et al. 1991, 1993; Tsong 1991; Teissié and Rols 1993; Gabriel and Teissié 1997; Maswiwat et al. 2008). In addition, a recent study suggests that this value can vary considerably even between cells of the same type (Towhidi et al. 2008).

All the experimental studies cited above investigated $\Delta\Psi_m$ and/or electroporation in single (isolated) cells. In actual situations, however, cells are rarely isolated and, when sufficiently close to each other, they also mutually distort the electric field around each other. Often, the cells are also in direct contact, forming two-dimensional (monolayers attached to the bottom of a dish) or three-dimensional (tissues) structures. Moreover, cells in these structures are often also interconnected (by channels, bridges, gap junctions, etc.).

Here, we first review some of the state-of-the-art methods for determining $\Delta\Psi_m$ and measuring electroporation-mediated molecular transport and then combine these methods to study the correlation between $\Delta\Psi_m$ and transport, measuring the two quantities on the same cells. Since the methods for determination of $\Delta\Psi_m$ differ substantially for regular and irregular cells and for single cells and those in clusters, we first describe each of these methods in some detail and then present their application on various cell shapes and formations. We study the correlation of $\Delta\Psi_m$ with electroporation-mediated transport both in isolated cells and in cells in clusters, with the latter revealing a more complex, field strength–dependent behavior.

Materials and Methods

For cells with sufficiently regular shapes (spheres, spheroids, cylinders) that are sufficiently far apart (dilute suspensions), $\Delta\Psi_m$ can be derived analytically. With irregular shapes and/or with cells close to each other, the analytical approach fails; but using modern computers and numerical methods, $\Delta\Psi_m$ induced on such cells can still be evaluated quite accurately. An alternative to both analytical and numerical determination is the experimental approach, which can be performed noninvasively using potentiometric dyes. In the first three subsections below, we treat each of these approaches separately. In the fourth subsection, we describe a method for monitoring the transport across the membrane.

Analytical Derivation of $\Delta\Psi_m$

The derivation of the induced component of transmembrane voltage is based on solving the following equation:

$$\nabla\left(\left(\sigma+\varepsilon\frac{\partial}{\partial t}\right)\nabla\Psi(x,y,z,t)\right)=0 \tag{1}$$

which characterizes the spatial and temporal distribution of the electric potential Ψ. For the steady-state situation, the time derivatives are equal to zero, and Eq. 1 simplifies to Laplace's equation:

$$\nabla\cdot\nabla\Psi(x,y,z)=0 \tag{2}$$

Solving this equation in a particular coordinate system and applying physically realistic boundary conditions (finiteness of Ψ, continuity of Ψ and its derivatives, asymptotic vanishing of the cell's effect on Ψ with increasing distance from the cell) yields the actual spatial distribution of Ψ. The induced transmembrane voltage is then calculated as the difference between the values of Ψ on both sides of the membrane:

$$\Delta\Psi_m=\Psi_{int}-\Psi_{ext} \tag{3}$$

For a single spherical cell with a nonconductive plasma membrane, Laplace's equation is solved in the spherical coordinate system, which leads to the formula often referred to as the steady-state Schwan equation (Pauly and Schwan 1959):

$$\Delta\Psi_m=1.5\,ER\cos\theta \tag{4}$$

where E is the external electric field, R is the cell radius and θ is the angle measured from the center of the cell with respect to the direction of the field. For exposures to a DC field lasting hundreds of microseconds or more, this formula can safely be applied to yield the maximal steady-state value of the induced transmembrane voltage on a single cell with a shape sufficiently close to a sphere. To describe also the transient behavior during the initial microseconds, one has to use the more general first-order Schwan equation (Pauly and Schwan 1959)

$$\Delta\Psi_m=1.5\,ER\cos\theta\left(1-e^{-t/\tau_m}\right) \tag{5a}$$

where t_m is the time constant of the membrane charging,

$$\tau_m = \frac{R\,\varepsilon_m}{2d\frac{\sigma_i\sigma_e}{\sigma_i+2\sigma_e} + R\sigma_m} \tag{5b}$$

with σ_i, σ_m and σ_e being the electric conductivities of the cytoplasm, cell membrane and extracellular medium, respectively; ε_m being the dielectric permittivity of the membrane; and d being the membrane thickness.

Equations 5a and 5b are applicable to exposures of spherical cells to sine (AC) electric fields with frequencies below 1 MHz and rectangular electric pulses longer than 1 μs. For even higher field frequencies and even shorter pulses, the second-order Schwan equation, in which the dielectric permittivities of the cytoplasm and the extracellular medium are also taken into account, must be used (Grosse and Schwan 1992; Kotnik et al. 1998; Kotnik and Miklavčič 2000b, 2006).

A sphere is a reasonable shape approximation for certain types of cells, particularly in suspensions; but many cells deviate from a spherical shape considerably. Other cell shapes that allow for analytical derivation of $\Delta\Psi_m$ are cylinders (e.g., muscle cells and axons of nerve cells), oblate spheroids (e.g., erythrocytes) and prolate spheroids (e.g., bacilli). To obtain the analogues of Schwan's equation for such cells, Laplace's equation is solved in a suitable coordinate system (Bernhard and Pauly 1973; Kotnik and Miklavčič 2000a; Gimsa and Wachner 2001). For a circular cylinder with the axis perpendicular to the field, this procedure yields

$$\Delta\Psi_m = 2\,ER\cos\theta \tag{6}$$

For an oblate (disk-shaped) spheroid with the axis of rotational symmetry aligned with the field, we get

$$\Delta\Psi_m = E\frac{R_2^2 - R_1^2}{\frac{R_2^2}{\sqrt{R_2^2-R_1^2}}\operatorname{arcctg}\frac{R_1}{\sqrt{R_2^2-R_1^2}} - R_1} \times \frac{R_2\cos\theta}{\sqrt{R_1^2\sin^2\theta + R_2^2\cos^2\theta}} \tag{7}$$

and for a prolate (cigar-shaped) spheroid with the axis of rotational symmetry aligned with the field,

$$\Delta\Psi_m = E\frac{R_1^2 - R_2^2}{R_1 - \frac{R_2^2}{\sqrt{R_1^2-R_2^2}}\ln\frac{R_1+\sqrt{R_1^2-R_2^2}}{R_2}} \times \frac{R_2\cos\theta}{\sqrt{R_1^2\sin^2\theta + R_2^2\cos^2\theta}} \tag{8}$$

where R_1 and R_2 are the radii of the spheroid in the directions parallel and perpendicular to the field, respectively. For spheroids rotated with their axis with respect to the field, the field vector is decomposed into the components parallel and perpendicular to the axis of the spheroid, and $\Delta\Psi_m$ is obtained as the combination of the voltages induced by the two components (Gimsa and Wachner 2001; Valič et al. 2003).

For nonspherical cells, it is generally more revealing to express $\Delta\Psi_m$ as a function of the arc length along the membrane than as a function of the angle θ (for a sphere, the two quantities are directly proportional). For uniformity, the normalized version of the arc length is used, denoted by p and increasing from 0 to 1 equidistantly along the arc of the membrane. Figures 1 and 2 show $\Delta\Psi_m(p)$ normalized to the cell size and electric field strength for an oblate and a prolate spheroid, respectively, with three different orientations with respect to the field.

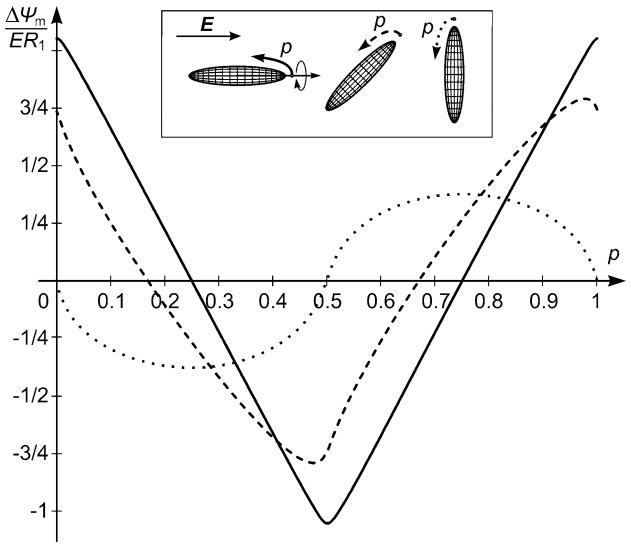

Fig. 1 Normalized steady-state $\Delta\Psi_m(p)$ as derived analytically for an oblate spheroidal cell with $R_2 = 5 \times R_1$ and with the axis of rotational symmetry aligned with the field (*solid*), at 45° with respect to the field (*dashed*) and perpendicular to the field (*dotted*)

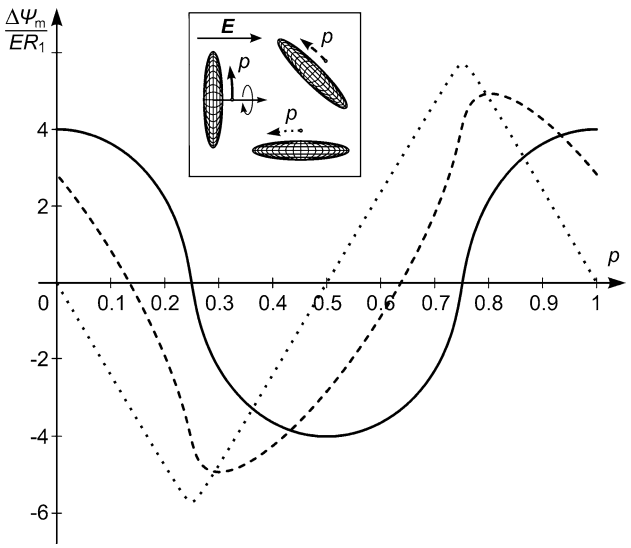

Fig. 2 Normalized steady-state $\Delta\Psi_m(p)$ as derived analytically for a prolate spheroidal cell with $R_2 = 0.2 \times R_1$ and with the axis of rotational symmetry aligned with the field (*solid*), at 45° with respect to the field (*dashed*) and perpendicular to the field (*dotted*)

Numerical Computation of $\Delta\Psi_m$

For cells for which $\Delta\Psi_m$ cannot be determined analytically—irregular cells as well as regular cells in dense suspensions and clusters—$\Delta\Psi_m$ can still be computed numerically, using either the finite-differences or finite-elements method. Here, we present the latter method, which is more suitable for handling irregularly shaped cells and formations (clusters) of such cells. Finite-elements computation of $\Delta\Psi_m$ is generally performed in four steps. First, the three-dimensional model of the cell(s) of interest is constructed. Second, the continuous geometry of the model and the differential equations describing the electric field are transformed into their discrete counterparts. Third, these equations are solved either directly or iteratively (until reaching adequate convergence) using the finite-elements method. Finally, values of the electric potential on both sides of the membrane are extracted from the computed data, and $\Delta\Psi_m$ is computed as their difference according to Eq. 3.

Below, we provide a short description of this method, focusing mainly on the most important aspects, while the reader familiar with the basics of finite-elements modeling will be able to implement this method by following the instructions provided in Pucihar et al. (2006, 2009a).

The three-dimensional model of an irregularly shaped cell can be constructed from a sequence of cross-sectional images of the cell under consideration. This model is then imported into a suitable numerical software package, such as COMSOL Multiphysics 3.4 (COMSOL, Burlington, MA), which discretizes the model into finite elements. The spatial and temporal distribution of the electric potential is computed by solving the discretized version of Eq. 1, with transmembrane electric current density, $J(t)$, given by the discretized version of

$$J(t) = \frac{\sigma_m(\Psi_{int}(t) - \Psi_{ext}(t))}{d} + \frac{\varepsilon_m}{d}\frac{\partial(\Psi_{int}(t) - \Psi_{ext}(t))}{\partial t} \tag{9}$$

with σ_m, ε_m, d, Ψ_i and Ψ_e having the same meanings as in Eqs. 3 and 5b. The first term on the right-hand side represents the conductive component and the second term, the capacitive component of the electric current flowing through the membrane.

Direct incorporation of a realistic cell membrane (a very thin layer of uniform thickness) would require the model to consist locally of an extremely large number of finite elements. However, unless the spatial distribution of the electric potential inside the membrane is of interest, this can be avoided. Namely, as far as Ψ_i and Ψ_e are concerned, the effect of a membrane with thickness d, electric conductivity σ_m and dielectric permittivity ε_m is equivalent to the effect of an interface with thickness 0, surface electric conductivity $\kappa_m = \sigma_m/d$ and surface dielectric permittivity $\beta_m = \varepsilon_m/d$. Thus, we can rewrite Eq. 9 as.

$$J(t) = \kappa_m(\Psi_i(t) - \Psi_e(t)) + \beta_m\frac{\partial(\Psi_i(t) - \Psi_e(t))}{\partial t} \tag{10}$$

The drop of electric potential at such an interface is equivalent to $\Delta\Psi_m$ induced on the membrane characterized by corresponding values of d, σ_m and ε_m. In models constructed in this way, the mesh of finite elements is easily generated as disproportionally small elements corresponding to the membrane interior are avoided (Pucihar et al. 2006, 2009a). Figure 3 shows normalized $\Delta\Psi_m(p)$ for two irregular cells attached to a flat surface.

In addition to irregular cells, numerical computation can be used for determination of $\Delta\Psi_m$ in cells in dense suspensions and in clusters. In dilute cell suspensions, the local field outside each cell is practically unaffected by other cells; and for spherical cells, the deviation of $\Delta\Psi_m$ from the prediction given by Eq. 4 is negligible. For suspensions with cell volume fractions over 10%, the distortion of the local field around each cell by the adjacent cells becomes more pronounced, $\Delta\Psi_m$ starts to deviate from Eq. 4 and its reliable determination requires numerical computation (Susil et al. 1998; Heida et al. 2002; Pavlin et al. 2002; Pucihar et al. 2007; Ying and Henriquez 2007). Figure 4 shows normalized $\Delta\Psi_m$ for an isolated spherical cell and for spherical cells in suspensions with three different cell volume fractions.

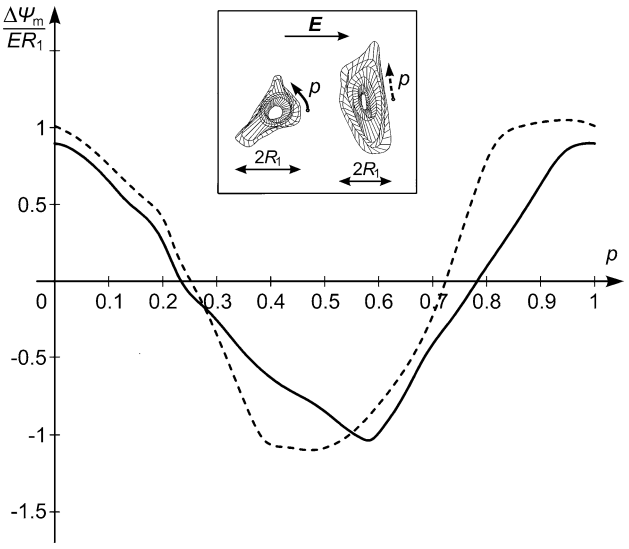

Fig. 3 Normalized steady-state $\Delta\Psi_m(p)$ as computed numerically for two irregularly shaped CHO cells growing on the flat surface of a cover glass

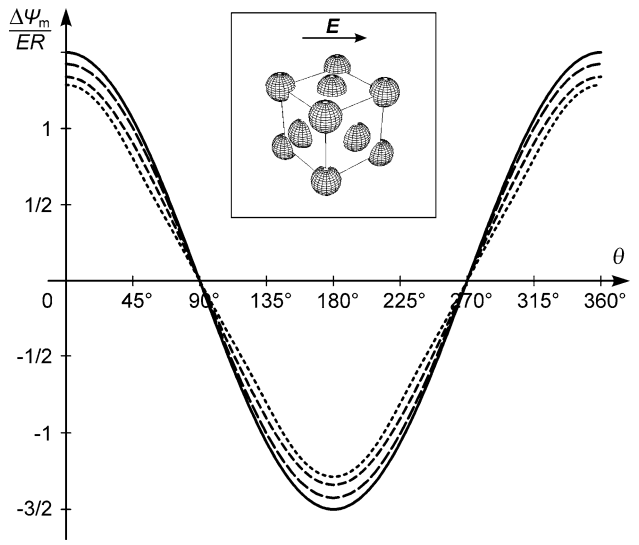

Fig. 4 Normalized steady-state $\Delta\Psi_m(\theta)$ as computed numerically for spherical cells in suspensions of various densities (intercellular distances). *Solid* The analytical result for a single cell as given by Eq. 4. *Dashed* Numerical results for cells arranged in a face-centered cubic lattice (shown in the *inset*) and occupying (with decreasing dash size) 10, 30 and 50% of the total suspension volume

Potentiometric Measurements of $\Delta\Psi_m$

An alternative to analytical and numerical determination of $\Delta\Psi_m$ are the experimental techniques. These include measurements with microelectrodes and with potentiometric fluorescent dyes. The invasive nature of microelectrodes, their low spatial resolution and physical presence, which distorts the external electric field, are considerable shortcomings. In contrast, measurements by means of potentiometric dyes are noninvasive, offer higher spatial resolution and do not distort the field and, thus, $\Delta\Psi_m$. As a consequence, the potentiometric dyes such as di-8-ANEPPS (Fluhler et al. 1985; Gross et al. 1986; Loew 1992; Pucihar et al. 2009b) have become the preferred tool in experimental studies and measurements of $\Delta\Psi_m$.

In water, di-8-ANEPPS is nonfluorescent but it incorporates into the lipid bilayer of the cell membrane, where it becomes strongly fluorescent, with fluorescence intensity varying proportionally to the change of $\Delta\Psi_m$ for voltages ranging from −280 to +250 mV (Lojewska et al. 1989; Cheng et al. 1999).

The protocol for staining the cells with di-8-ANEPPS is presented in detail, also in a video format, in Pucihar et al. (2009b). In brief, determination of $\Delta\Psi_m$ starts with 10-min incubation of the cells with 30 μM di-8-ANEPPS and 0.05% of pluronic acid (both Invitrogen, Eugene, OR), after which the cells are washed to remove the nonbound dye and pluronic acid. The cells are then exposed to the electric field, and a pair of images is acquired: a control image immediately before the exposure and a pulse image during the exposure. The excitation wavelength is set at 490 nm and emission is detected at 605 nm.

In the results presented here, we used Chinese hamster ovary (CHO-K1) cells plated in Lab-Tek II chambers (Nalge Nunc, Wiesbaden, Germany) at 0.7×10^5 cells/ml in HAM-F12 culture medium supplemented with 8% fetal calf serum, 0.15 mg/ml L-glutamine, 16 mg/ml gentamicin (all from Sigma-Aldrich, Steinheim, Germany) and 200 units/ml crystacillin (Pliva, Zagreb, Croatia) and incubated in 5% CO_2 at 37°C.

Before exposure to the electric field, the culture medium was replaced by a Spinner modification (calcium-depleted version) of minimum essential medium (SMEM, M8167 or M4767; Sigma-Aldrich). The imaging system consisted of a fluorescence microscope (AxioVert 200; Zeiss, Oberkochen, Germany) equipped with an oil immersion objective (×63, NA 1.4), a monochromator (Polychrome IV; Visitron, Puchheim, Germany), a 605-nm band-pass filter (605/55 m Chroma, Rockingham, VT) and a cooled CCD camera (VisiCam 1280, Visitron). $\Delta\Psi_m$ was measured for exposure to a single 50-ms pulse, 100 V/cm; these pulse parameters cause negligible heating, never result in electroporation and yield a sufficient signal-to-noise ratio for accurate and reproducible potentiometric measurements. Images were acquired and processed using the MetaMorph 7.1.1 software package (Molecular Devices, Downingtown, PA). Image acquisition lasted 50 ms and was synchronous with the pulse delivery (synchronization is a feature of the MetaMorph software).

After the acquisition, the acquired image must be processed in several steps. First, the background fluorescence is subtracted from both the pulse and control images. For the cell under investigation, the region of interest corresponding to the membrane is determined and the fluorescence intensities along this region in the pulse and control image are measured. For each pulse, the control data are then subtracted from the pulse data, and the result is divided by the control data to obtain the relative fluorescence changes. Finally, the relative fluorescence changes are transformed into values of $\Delta\Psi_m$ using a calibration curve. For more details on image acquisition and processing procedures, see Pucihar et al. (2006, 2009b).

Figure 5 shows $\Delta\Psi_m$ determined in this manner on an irregular cell attached to a flat surface.

Monitoring of Molecular Transport

To monitor transmembrane molecular transport and thereby determine the electroporated regions of the membrane, cells are exposed to the electroporating field in the presence of an otherwise membrane-impermeant fluorescent dye such as propidium iodide (PI). The fluorescence of

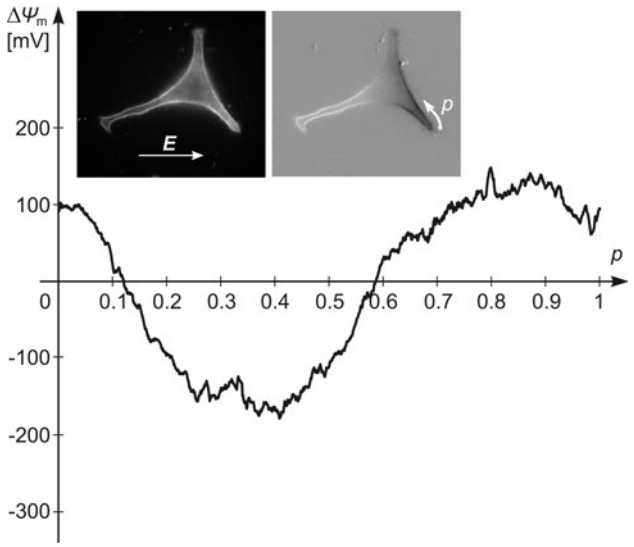

Fig. 5 Steady-state $\Delta\Psi_m(p)$ as measured potentiometrically using di-8-ANEPPS. *Left inset* Raw fluorescence image of a CHO cell stained with di-8-ANEPPS. *Right inset* Processed image. *Plot* $\Delta\Psi_m(p)$ determined from the processed image

PI increases by several orders of magnitude when the dye is bound to proteins and nucleic acids, due to which the localized entry of the dye through electroporated regions of the membrane into the cell is detected as a local increase in fluorescence.

Before exposure to an electroporating electric field, PI (Sigma, St. Louis, MO) is added to the medium in a quantity leading to a 100 μM concentration. The excitation wavelength is set at 530 nm and emission is detected at 605 nm.

In our experiments, electroporation-mediated transport was monitored on the same cells on which $\Delta\Psi_m$ was previously determined. Electroporation was induced by exposure to a single pulse, with durations ranging from 200 μs to 1.5 ms and amplitudes of 650–1,000 V/cm. Different parameters of porating pulses were deliberately chosen for different experiments to illustrate that our observations are valid over a range of porating pulses, i.e., to establish a proof of principle. The details on culturing, preparation, exposure, imaging of cells and image processing are given in the preceding subsection.

To verify whether the cells in a monolayer were interconnected, we used the scrape-loading test, described in detail in El-Fouly et al. (1987). The culture medium was supplemented by 1 mM lucifer yellow (Sigma-Aldrich), a membrane-impermeant fluorescent dye. The tip of a needle was used to scrape the cells in the monolayer, which allows lucifer yellow to enter the scraped cells and subsequently the adjacent intact cells provided that they were connected to the scraped ones. After 5 min of incubation, the dye was washed away with pure medium, and intracellular fluorescence was observed with the imaging system described above. The dye was excited with 425 nm and emission was detected at 605 nm.

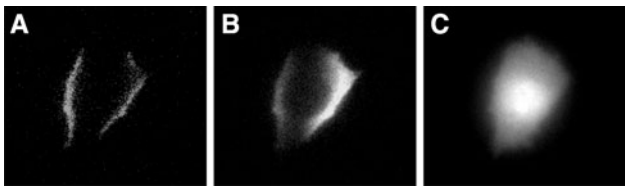

Fig. 6 A sequence of images showing PI fluorescence at **a** 200 ms, **b** 2 s and **c** 3 min after exposure to a single 100-μs, 1,000-V/cm rectangular electric pulse. Images reveal diffusion of PI through electroporated regions of the membrane (**a**), into the cytosol (**b**) and finally into the nucleus (**c**) of a CHO cell

Figure 6 shows three consecutive images of molecular transport into an electroporated cell.

Results and Discussion

Isolated Spherical Cells

Cells in suspension typically resemble a sphere sufficiently well as to allow for accurate description of $\Delta\Psi_m$ by means of Schwan's equations—Eq. 5a to describe the transient process of $\Delta\Psi_m$ formation and Eq. 4 for the steady state of $\Delta\Psi_m$. This is also the case for CHO cells used in our study (see Fig. 7a).

Figure 7a shows a processed image of di-8-ANEPPS fluorescence for a spherical CHO cell exposed to a 50-ms, 100-V/cm electric pulse. With this pulse duration, the signal-to-noise ratio was sufficient for accurate measurements by our system, while the pulse amplitude was low enough to avoid electroporation. The left hemisphere of the cell, where $\Delta\Psi_m$ is negative, appears bright and the right hemisphere, with positive $\Delta\Psi_m$, is dark. Figure 7b displays the flow of PI into this same cell when exposed to a 1.5-ms, 650-V/cm electric pulse, reflecting the electroporated regions of the membrane. The solid curve in Fig. 7c shows the spatial distribution of $\Delta\Psi_m$ as measured from di-8-ANEPPS fluorescence (left *y* scale), while the dashed curve corresponds to the analytical prediction of $\Delta\Psi_m$ given by Eq. 4 for the nonelectroporating 100-V/cm pulse used in Fig. 7a ($\Delta\Psi_m^{(A)}$, left *y* scale) and for the electroporating 650-V/cm pulse used in Fig. 7b ($\Delta\Psi_m^{(B)}$, right *y* scale). Comparison between the solid and dashed curves (using the left *y* scale) shows good agreement between the measurement and theory for the 100-V/cm pulse, while the theoretical prediction for the 650-V/cm (dashed curve using the right *y* scale) is valid only until the onset of electroporation, which causes a significant decrease of the local $\Delta\Psi_m$. Figure 7d quantifies the PI fluorescence from Fig. 7b measured along the same path.

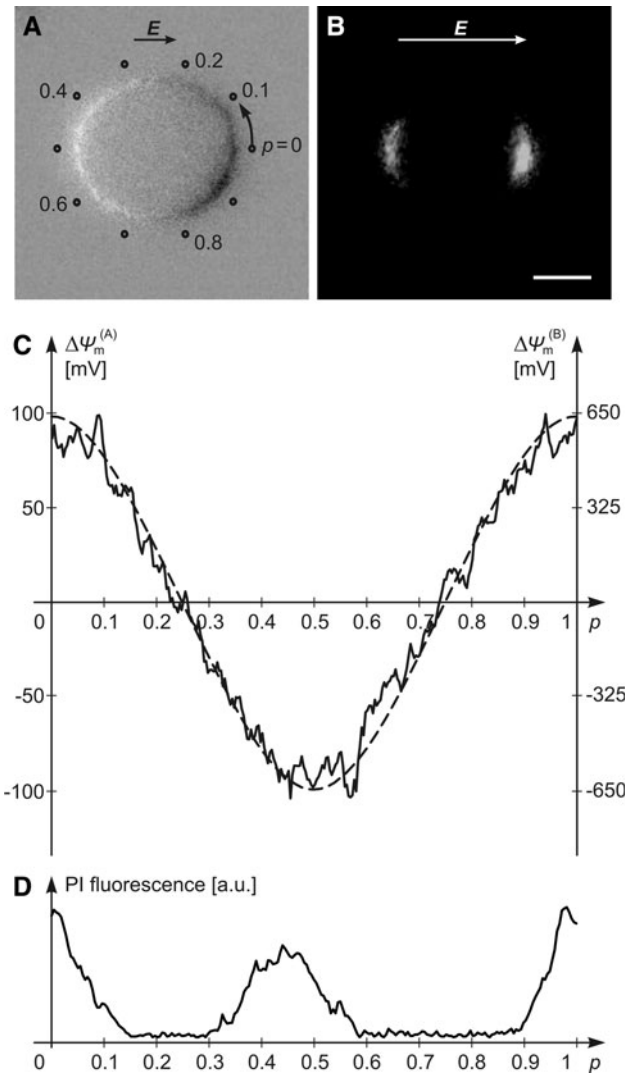

Fig. 7 Steady-state $\Delta\Psi_m(p)$ and electroporation of a spherical CHO cell. **a** Changes in fluorescence of di-8-ANEPPS caused by a nonporating 50-ms, 100-V/cm pulse. **b** Transport of PI into the same cell caused by a porating 1.5-ms, 650-V/cm pulse, as visualized 200 ms after exposure. Bar = 5 µm. **c** Steady-state $\Delta\Psi_m(p)$ measured along the path shown in (**a**) (*solid*), as predicted by Eq. 4 (*dashed*). The left *y* scale corresponds to the 100-V/cm pulse amplitude used in (**a**) and the right *y* scale, to the 650-V/cm used in (**b**). **d** PI fluorescence measured along the path shown in (**a**)

The experimental results in Fig. 7 confirm the theoretical prediction that the highest values of $\Delta\Psi_m$ are found in the membrane regions facing the electrodes (the "poles" of the cell) and show that electroporation-mediated transport is detected in these same regions, i.e., the areas for which the absolute value of $\Delta\Psi_m$ is the highest. From the location of electroporated regions in Fig. 7b and from the curve of $\Delta\Psi_m^{(B)}$ in Fig. 7c it would follow that with the applied pulse parameters electroporation is detectable for $\Delta\Psi_m$ exceeding ~480 mV (i.e., $\Delta\Psi_m \approx 480$ mV at the edge of the transport region). However, since electroporation distorts $\Delta\Psi_m$ (Hibino et al. 1991, 1993), the stated value is only a rough estimate. Moreover, the threshold of uptake detection also depends on the sensitivity of the imaging system (Gabriel and Teissié 1999; Pucihar et al. 2008) and generally on the dye being used for detection of molecular transport (He et al. 2007). Figure 7d confirms the observed correlation between above-threshold $\Delta\Psi_m$ and detectable uptake.

Isolated Irregularly Shaped Cells

Cells growing in tissues in vivo or in a dish in vitro have markedly irregular shapes, and $\Delta\Psi_m$ on such cells cannot be determined analytically. In other words, for regular cell shapes $\Delta\Psi_m$ can be expressed by elementary functions such as the ones given by Eqs. 4–8, but for irregular shapes this is impossible. As a consequence, numerical and experimental methods are used for this purpose. In analogy to Fig. 7, Fig. 8 shows good agreement between the measured and the numerically computed $\Delta\Psi_m$ and confirms that also in irregular cells electroporation occurs in the membrane regions with the highest absolute value of $\Delta\Psi_m$, i.e., the regions facing the electrodes. This is most obvious in cells with pronounced protrusions, where with increase of field strength electroporation first becomes detectable at the very tips of these protrusions (Teruel and Meyer 1997).

The results shown in Figs. 7, 8 confirm the finding that electroporation is limited to the membrane regions in which the absolute value of $\Delta\Psi_m$ exceeds a certain critical level. In Fig. 7, this level was at ~480 mV, while in Fig. 8 it is about ~ 650 mV. This reflects the fact that the "threshold" of detectable electroporation depends on, in addition to the molecules being introduced and sensitivity of the imaging system, pulse duration (1.5 ms in Fig. 7, and 200 µs in Fig. 8). Moreover, in Fig. 8, the large amplitude of the pulse, and consequently of $\Delta\Psi_m$, resulted in extensive electroporation, covering a much larger fraction of the membrane area than in Fig. 7.

It should be noted that while the spatial distribution of $\Delta\Psi_m$ expressed as a function of the normalized arc length, $\Delta\Psi_m(p)$, is fairly similar for many cells ranging from spherical to very irregular shapes (see, e.g., Figs. 3, 8), their plots of $\Delta\Psi_m$ when expressed as a function of the polar angle, $\Delta\Psi_m(\theta)$, can differ from each other quite substantially. For spherical cells, $\Delta\Psi_m(p)$ and $\Delta\Psi_m(\theta)$ are equivalent (as in this case $p = \theta/360°$), while for some highly irregular shapes (e.g., cells with curved protrusions), $\Delta\Psi_m(\theta)$ cannot even be defined unambiguously.

Cells in Dense Suspensions and in Monolayers

In dilute cell suspensions, the distance between cells is much larger than the cells themselves and the local field outside each cell is practically unaffected by the presence

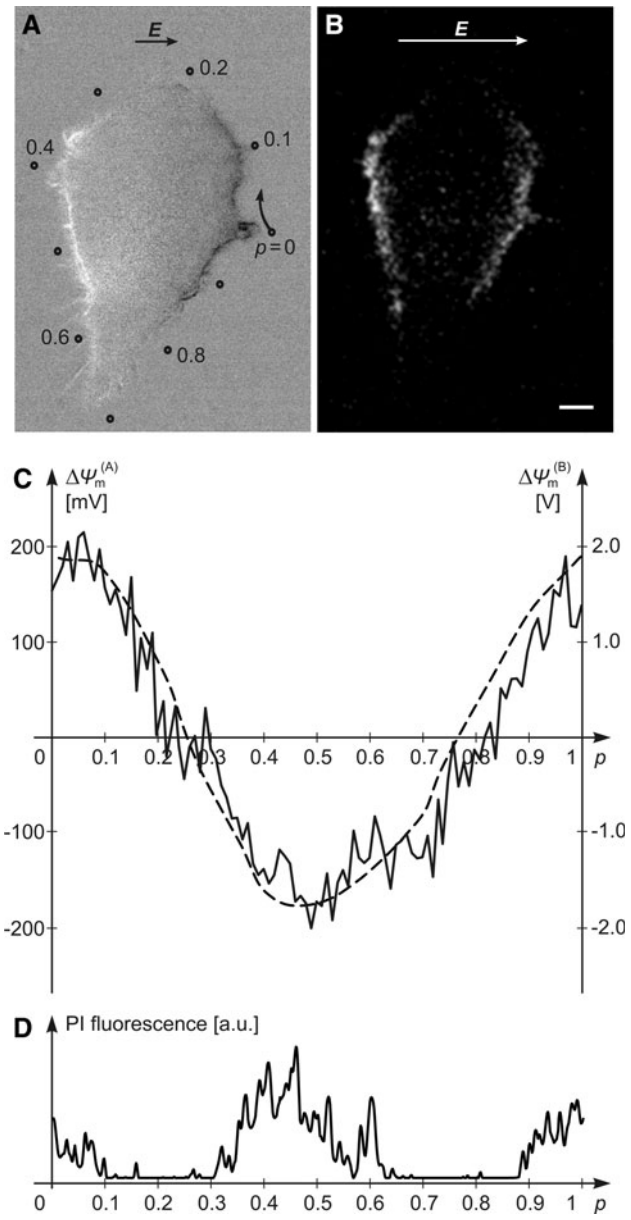

Fig. 8 Steady-state $\Delta\Psi_m(p)$ and electroporation of an irregular CHO cell. **a** Changes in fluorescence of di-8-ANEPPS caused by a nonporating 50-ms, 100-V/cm pulse. **b** Transport of PI into the same cell caused by a porating 200-µs, 1,000-V/cm pulse, as visualized 200 ms after exposure. Bar = 5 µm. **c** Steady-state $\Delta\Psi_m(p)$ measured along the path shown in (**a**) (*solid*) and as predicted by numerical computation (*dashed*). The left *y* scale corresponds to the 100-V/cm pulse amplitude used in (**a**) and the right *y* scale, to the 1,000-V/cm used in (**b**). **d** PI fluorescence measured along the path shown in (**a**)

of other cells. Thus, for cells representing <1% of the suspension volume (for a spherical cell with a radius of 10 µm, this means up to ~2 million cells/ml), the deviation of $\Delta\Psi_m(\theta)$ from the prediction of the steady-state Schwan's equation as given by Eq. 4 is insignificant. However, for larger volume fractions occupied by the cells, the distortion of the local field around each cell by the adjacent cells becomes more pronounced. As the volume fraction occupied by the cells increases beyond 10%, $\Delta\Psi_m(\theta)$ starts to deviate from that given by Eq. 4 as the factor 1.5 gradually decreases toward 1 and the spatial distribution also starts to diverge from the cosine function, as shown in Fig. 4 (Susil et al. 1998; Pavlin et al. 2002). Due to the lower $\Delta\Psi_m$, with the same pulse parameters the efficiency of electroporation is typically lower in dense suspensions than in dilute ones (Pucihar et al. 2007).

For even larger volume fractions, the cells come into direct contact, and the electrical properties of the suspension start to resemble those of a tissue but only to a certain extent. Namely, cells can form specific structures, such as layers; and they can be interconnected through intercellular pathways (e.g., gap junctions). The amplitude and spatial distribution of $\Delta\Psi_m$ in these cells can differ considerably from those observed in single isolated cells. This is because dense cell packing shields the cells electrically to some extent, while intercellular pathways can connect adjacent cells electrically. Due to the nature of the tissue structure, it is difficult to observe these effects experimentally on the level of an individual tissue cell. One such study combined numerical modeling and experiments to estimate the critical values of $\Delta\Psi_m$ on a single cell in liver tissue (Miklavčič et al. 2000). As a more feasible alternative, we can study clusters of cells growing in monolayers, which present a simple model for examining the behavior of cells in tissues. As in tissues, cells in such clusters also have complex geometric shapes, are densely packed and are often interconnected. Thus, the only significant difference is the two-dimensional arrangement of a monolayer as opposed to a typically three-dimensional cellular structure of a tissue.

Intercellular pathways provide the passages for exchange of ions between neighboring cells. The opened or closed state of these passages renders the cells electrically connected or insulated, respectively; and in this manner it can affect both $\Delta\Psi_m$ and electroporation considerably.

Figure 9 displays the results of the scrape-loading test on CHO cells growing in a monolayer attached to a cover

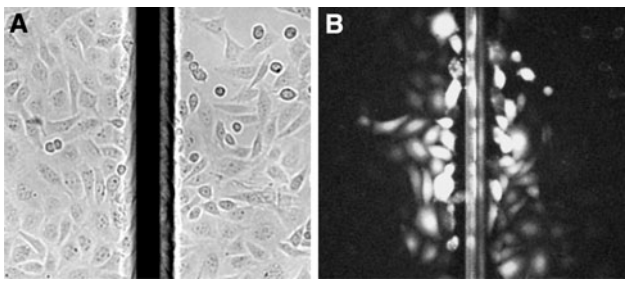

Fig. 9 Scrape-loading test on CHO cells performed with 1 mM lucifer yellow. **a** Phase-contrast image of cells scraped with a needle (*black vertical in the middle*). **b** Fluorescence of cells 5 min later. The dye entered the damaged cells and quickly diffused into the neighboring, undamaged cells

glass. The molecules of lucifer yellow introduced into the scraped cells quickly diffuse into adjacent cells, which demonstrates that these cells are interconnected.

Figure 10 shows $\Delta\Psi_m$ and electroporation of a pair of such CHO cells. With a nonelectroporating pulse, $\Delta\Psi_m$ induced on the cell membranes was continuous when traced along the outer boundary of the pair (Fig. 10c, solid curve). This is in good agreement with the numerically computed $\Delta\Psi_m$ for the case of electrically interconnected cells (Fig. 10c, dashed black). In other words, for the electric field of 100 V/cm, the pair of cells behaved as if it were one big cell, reflecting the presence of intercellular pathways, which is also demonstrated in Fig. 9 for the case where no field is present. A similar general observation, but without a quantitative assessment, was reported before by other authors (Gross et al. 1986; Hassan et al. 2002).

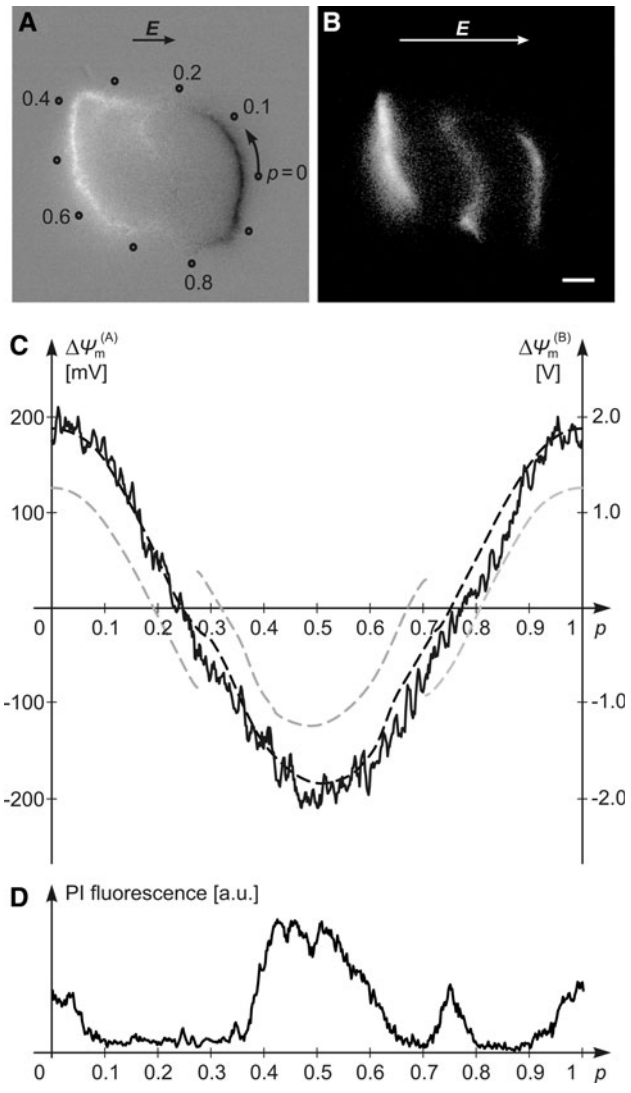

Fig. 10 Steady-state $\Delta\Psi_m(p)$ and electroporation of a pair of connected CHO cells. **a** Changes in fluorescence of di-8-ANEPPS caused by a nonporating 50-ms, 100-V/cm pulse. **b** Transport of PI into the same two cells caused by a porating 200-µs, 1,000-V/cm pulse, as visualized 200 ms after exposure. Bar in **b** = 5 µm. **c** Steady-state $\Delta\Psi_m(p)$ measured along the path shown in (**a**) (*solid*) and as computed numerically for electrically interconnected (*dashed black*) and electrically insulated (*dashed gray*) cells. The left *y* scale corresponds to the 100-V/cm pulse amplitude used in (**a**) and the right *y* scale, to the 1,000-V/cm used in (**b**). **d** PI fluorescence measured along the path shown in **a**

When the same pair of CHO cells was exposed to a field of 1,000 V/cm leading to electroporation, however, molecular transport occurred in the membrane regions for which numerical computations predicted the highest $\Delta\Psi_m$ if the cells were modeled as electrically insulated (Fig. 10c, dashed gray). In other words, each cell in the pair was electroporated individually. This is partly also seen in Fig. 10d as a peak in fluorescence at $0.7 < p < 0.8$ that reflects electroporation of the cell at the right, in the region in which $\Delta\Psi_m$ would be close to zero if the two cells were electrically connected (Fig. 10c, dashed black). These results suggest that with $\Delta\Psi_m$ substantially above physiological levels, the intercellular pathways are blocked. This is in general agreement with the finding that some of these pathways, e.g., gap junctions, are voltage-gated (Harris et al. 1981; Bukauskas et al. 1995; Valiunas et al. 1997; Qu and Dahl 2002; Yeager and Harris 2007). Still, as voltage gating has been demonstrated only for exposures longer than several milliseconds, while our electroporating pulse lasted only 200 µs, it remains to be verified that (1) the intercellular connections in CHO cells are of the voltage-gated type and (2) voltage gating can occur so rapidly.

Conclusion

By combining experimental measurements with theoretical predictions, we confirm that in isolated cells of both regular and irregular shapes, electroporation-mediated transport is confined to the membrane regions with the highest absolute values of $\Delta\Psi_m$. For isolated cells, the theoretical predictions are straightforward, while in clusters, they require additional information regarding the electrical properties of the contact surfaces between cells. In other words, it must be known whether the cells are electrically interconnected or not. Our results suggest that this question might not have an unambiguous answer as the cells in clusters seem to behave differently when exposed to different field strengths—namely, the localization of transport through electroporated membrane regions implies that at field strengths sufficient for electroporation, cells behave as electrically insulated. In contrast, with substantially weaker, nonelectroporating fields, potentiometric measurements show that the cells in these same clusters behave as electrically interconnected. These results suggest that sufficiently high electric fields affect the intercellular

pathways and thus alter the electric behavior of the cells with respect to their normal physiological state.

Acknowledgement This work was supported by the Slovenian Research Agency (project Z2-9227 and program P2-0249). We dedicate this report to the memory of Robert Susil.

References

Alberts B, Johnson A, Lewis J et al (2008) Molecular biology of the cell, 5th edn. Garland Science, New York, pp 669–671

Bernhard J, Pauly H (1973) Generation of potential differences across membranes of ellipsoidal cells in an alternating electrical field. Biophysik 10:89–98

Bukauskas FF, Elfgang C, Willecke K et al (1995) Biophysical properties of gap junction channels formed by mouse connexin40 in induced pairs of transfected human HeLa cells. Biophys J 68:2289–2298

Cheng DKL, Tung L, Sobie EA (1999) Nonuniform responses of transmembrane potential during electric field stimulation of single cardiac cells. Am J Physiol Heart Circ Physiol 277:H351–H362

El-Fouly MH, Trosko JE, Chang CC (1987) Scrape-loading and dye transfer: a rapid and simple technique to study gap junctional intercellular communication. Exp Cell Res 168:422–430

Escoffre JM, Portet T, Wasungu L et al (2009) What is (still not) known of the mechanism by which electroporation mediates gene transfer and expression in cells and tissues. Mol Biotechnol 41:286–295

Fluhler E, Burnham VG, Loew LM (1985) Spectra, membrane binding, and potentiometric responses of new charge shift probes. Biochemistry 24:5749–5755

Gabriel B, Teissié J (1997) Direct observation in the millisecond time range of fluorescent molecule asymmetrical interaction with the electropermeabilized cell membrane. Biophys J 73:2630–2637

Gabriel B, Teissié J (1999) Time courses of mammalian cell electropermeabilization observed by millisecond imaging of membrane property changes during the pulse. Biophys J 76:2158–2165

Gimsa J, Wachner D (2001) Analytical description of the transmembrane voltage induced on arbitrarily oriented ellipsoidal and cylindrical cells. Biophys J 81:1888–1896

Gross D, Loew LM, Webb W (1986) Optical imaging of cell membrane potential changes induced by applied electric fields. Biophys J 50:339–348

Grosse C, Schwan HP (1992) Cellular membrane potentials induced by alternating fields. Biophys J 63:1632–1642

Harris AL, Spray DC, Bennett MVL (1981) Kinetic properties of a voltage-dependent junctional conductance. J Gen Physiol 77:95–117

Hassan N, Chatterjee I, Publicover NG et al (2002) Mapping membrane-potential perturbations of chromaffin cells exposed to electric fields. IEEE Trans Plasma Sci 30:1516–1524

He H, Chang DC, Lee YK (2007) Using a micro electroporation chip to determine the optimal physical parameters in the uptake of biomolecules in HeLa cells. Bioelectrochemistry 70:363–368

Heida T, Wagenaar JBM, Rutten WLC, Marani E (2002) Investigating membrane breakdown of neuronal cells exposed to nonuniform electric fields by finite-element modeling and experiments. IEEE Trans Biomed Eng 49:1195–1203

Hibino M, Shigemori M, Itoh H et al (1991) Membrane conductance of an electroporated cell analyzed by submicrosecond imaging of transmembrane potential. Biophys J 59:209–220

Hibino M, Itoh H, Kinosita K Jr (1993) Time courses of cell electroporation as revealed by submicrosecond imaging of transmembrane potential. Biophys J 64:1789–1800

Hu Q, Joshi RP (2009) Transmembrane voltage analyses in spheroidal cells in response to an intense ultrashort electrical pulse. Phys Rev E 79:11901

Kennedy SM, Ji Z, Hedstrom JC et al (2008) Quantification of electroporative uptake kinetics and electric field heterogeneity effects in cells. Biophys J 94:5018–5027

Kotnik T, Miklavčič D (2000a) Analytical description of transmembrane voltage induced by electric fields on spheroidal cells. Biophys J 79:670–679

Kotnik T, Miklavčič D (2000b) Second-order model of membrane electric field induced by alternating external electric fields. IEEE Trans Biomed Eng 47:1074–1081

Kotnik T, Miklavčič D (2006) Theoretical evaluation of voltage inducement on internal membranes of biological cells exposed to electric fields. Biophys J 90:480–491

Kotnik T, Bobanović F, Miklavčič D (1997) Sensitivity of transmembrane voltage induced by applied electric fields—a theoretical analysis. Bioelectrochem Bioenerg 43:285–291

Kotnik T, Miklavčič D, Slivnik T (1998) Time course of transmembrane voltage induced by time-varying electric fields—a method for theoretical analysis and its application. Bioelectrochem Bioenerg 45:3–16

Lodish H, Berk A, Kaiser CA et al (2008) Molecular cell biology, 6th edn. WH Freeman, New York, pp 458–460

Loew LM (1992) Voltage sensitive dyes: measurement of membrane potentials induced by DC and AC electric fields. Bioelectromagn Suppl 1:179–189

Lojewska Z, Franks DL, Ehrenberg B et al (1989) Analysis of the effect of medium and membrane conductance on the amplitude and kinetics of membrane potentials induced by externally applied electric fields. Biophys J 56:121–128

Maswiwat K, Wachner D, Gimsa J (2008) Effects of cell orientation and electric field frequency on the transmembrane potential induced in ellipsoidal cells. Bioelectrochemistry 74:130–141

Miklavčič D, Šemrov D, Mekid H et al (2000) A validated model of in vivo electric field distribution in tissues for electrochemotherapy and for DNA electrotransfer for gene therapy. Biochim Biophys Acta 1523:73–83

Neumann E, Rosenheck K (1972) Permeability changes induced by electric impulses in vesicular membranes. J Membr Biol 10:279–290

Pauly H, Schwan HP (1959) Über die Impedanz einer Suspension von kugelformigen Teilchen mit einer Schale. Z Naturforsch B 14:125–131

Pavlin M, Pavšelj N, Miklavčič D (2002) Dependence of induced transmembrane potential on cell density, arrangement, and cell position inside a cell system. IEEE Trans Biomed Eng 49:605–612

Pucihar G, Kotnik T, Valič B et al (2006) Numerical determination of transmembrane voltage induced on irregularly shaped cells. Ann Biomed Eng 34:642–652

Pucihar G, Kotnik T, Teissié J et al (2007) Electroporation of dense cell suspensions. Eur Biophys J 36:173–185

Pucihar G, Kotnik T, Miklavčič D et al (2008) Kinetics of transmembrane transport of small molecules into electropermeabilized cells. Biophys J 95:2837–2848

Pucihar G, Miklavčič D, Kotnik T (2009a) A time-dependent numerical model of transmembrane voltage inducement and electroporation of irregularly shaped cells. IEEE Trans Biomed Eng 56:1491–1501

Pucihar G, Kotnik T, Miklavčič D (2009b) Measuring the induced membrane voltage with di-8-ANEPPS. J Vis Exp 33:1659

Qu Y, Dahl G (2002) Function of the voltage gate of gap junction channels: selective exclusion of molecules. Proc Natl Acad Sci USA 99:697–702

Susil R, Šemrov D, Miklavčič D (1998) Electric field induced transmembrane potential depends on cell density and organization. Electro Magnetobiol 17:391–399

Teissié J, Rols MP (1993) An experimental evaluation of the critical potential difference inducing cell membrane electropermeabilization. Biophys J 65:409–413

Teissié J, Golzio M, Rols MP (2005) Mechanisms of cell membrane electropermeabilization: a minireview of our present (lack of?) knowledge. Biochim Biophys Acta 1724:270–280

Tekle E, Astumian RD, Chock PB (1994) Selective and asymmetric molecular-transport across electroporated cell-membranes. Proc Natl Acad Sci USA 91:11512–11516

Teruel MN, Meyer T (1997) Electroporation-induced formation of individual calcium entry sites in the cell body and processes of adherent cells. Biophys J 73:1785–1796

Towhidi L, Kotnik T, Pucihar G et al (2008) Variability of the minimal transmembrane voltage resulting in detectable membrane electroporation. Electromagn Biol Med 27:372–385

Tsong TY (1991) Electroporation of cell membranes. Biophys J 60:297–306

Valič B, Golzio M, Pavlin M et al (2003) Effect of electric field induced transmembrane potential on spheroidal cells: theory and experiment. Eur Biophys J 32:519–528

Valiunas V, Bukauskas FF, Weingart R (1997) Conductances and selective permeability of connexin43 gap junction channels examined in neonatal rat heart cells. Circul Res 80:708–719

Weaver JC (2003) Electroporation of biological membranes from multicellular to nano scales. IEEE Trans Diel El Insul 10:754–768

Yeager M, Harris AL (2007) Gap junction channel structure in the early 21st century: facts and fantasies. Curr Opin Cell Biol 19:521–528

Ying W, Henriquez CS (2007) Hybrid finite element method for describing the electrical response of biological cells to applied fields. IEEE Trans Biomed Eng 54:611–620